Point-spread functions of a polarizing microscope equipped with high-numerical-aperture lenses

Rudolf Oldenbourg and Peter Török

In an effort to establish the imaging properties of a new type of polarized-light microscope, we recorded images of small, uniaxial, birefringent crystals. We show that the sequence of in-focus and out-of-focus images, the so-called point-spread function, of a submicroscopic crystal can be used to measure the orientation of its optic axis in three-dimensional space. By analogy to conoscopic images out-of-focus images reveal the changes in relative phase shift between the extraordinary and the ordinary rays that propagate at different directions through the crystal. We also present simulated images of a pointlike anisotropic scattering particle and compare these with our experimental findings. The theoretical model is based on a complete vectorial theory for partial coherent imaging by use of polarized light and high-numerical-aperture lenses.

OCIS codes: 180.6900, 120.2130, 260.1440, 180.3170, 050.1940.

1. Introduction

The polarized-light microscope (PLM) has the unique potential to measure the alignment of molecular bonds and fine-structure form that lead to optical anisotropy, such as birefringence and dichroism. Recent advances in electronic imaging, digital image processing, and electro-optic devices for modulating the polarization of light have lead to new instrumentation that can measure the parameters of optical anisotropy quickly and at many specimen points simultaneously.[1–5] However, to exploit fully the improved instrumentation, we need to better understand the imaging properties of the polarizing microscope, such as the evolution of the images of a small birefringent particle when it is brought into and out of focus.

In this paper, we report measurements of so-called point-spread functions by using images of uniaxial birefringent calcite crystals. Although the point-spread functions of fluorescent objects have been studied extensively,[6–9] we believe this is the first report of a systematic evaluation of optical sections of small birefringent crystals. The crystals were observed with a new type of PLM (the Pol-Scope[10]) that is equipped with high-numerical-aperture (high-NA) lenses. Pol-Scope images are two-dimensional maps of the polarization orientation and the relative phase shift of the ordinary (o) and the extraordinary (e) rays that form individual image points. Using calcite crystals large enough to be able to resolve their morphology, we demonstrate that Pol-Scope images of crystals that are placed out of focus reveal the orientation of the crystal's optic axis in three-dimensional (3-D) space. We go on to show that submicroscopic calcite crystals whose morphology cannot be resolved with the light microscope produce out-of-focus images that have features similar to those of larger crystals. By analogy to larger crystals these features reveal the 3-D orientation of the optic axis of submicroscopic crystals.

To aid in the interpretation of the experimental observations, we calculated images of anisotropic point scatterers by using a recently developed theory for partial coherent imaging with polarized light and high-NA lenses.[11] We find good agreement between theory and experiment for in-focus images of small anisotropic particles. Thus combining in-focus and out-of-focus images allows the birefringence retardation and optic-axis orientation of small, unresolved, birefringent particles to be determined in 3-D space. The observation of small crystals and the measurement and the analysis of their point-spread functions, as presented here, will serve us in the future to establish restoration procedures for Pol-Scope optical

R. Oldenbourg (rudolfo@mbl.edu) is with the Marine Biological Laboratory, Woods Hole, Massachusetts 02543. P. Török is with the Department of Engineering Science, Oxford University, Oxford OX1 3PJ, UK.

Received 4 May 2000; revised manuscript received 16 August 2000.

0003-6935/00/346325-07$15.00/0

sections recorded from complex 3-D objects, such as living cells.

2. Materials and Methods

A. Preparation of Calcite Crystals

Calcite crystals were prepared by the mixing, in approximate stochiometric amounts, of saturated aqueous solutions of sodium bicarbonate and calcium chloride. On mixing a white precipitate of calcite crystals formed. A small amount of solution and precipitate was transferred to a microscope coverglass. We washed away the solution, which contained unreacted amounts of the original compounds, by rinsing the coverglass with purified water. Crystals that adhered to the coverglass were allowed to dry and were then embedded in Permount (all chemicals were obtained from Fisher Scientific). The coverglass was placed on a microscope slide so that the crystals and the Permount were sandwiched between them. The Permount was cured to form a mechanically stable assembly that had a uniform refractive index of 1.52 with calcite crystals suspended in the middle.

Calcite is a negatively birefringent, uniaxial crystal. The refractive index for *o* rays that are polarized perpendicular to the optic axis is 1.6584, and for *e* rays that are polarized parallel to the optic axis it is 1.4864. Hence the birefringence is $\Delta n = n_e - n_o = -0.172$ (see, e.g., Ref. 12).

B. Birefringence Imaging

We imaged calcite crystals by using a new type of PLM.[10,13] In brief, the optical design of the new Pol-Scope builds on the traditional PLM with two essential modifications: (1) the specimen is illuminated with nearly circularly polarized light, and (2) the compensator is replaced by two electro-optic modulators. The modulators are made from liquid-crystal devices that function as variable linear retarders. Their slow axes are permanently adjusted at an angle of 45° to each other. Although their axes are fixed, varying the voltage applied to each liquid crystal can change the magnitude of retardance. This combination of two variable retarders can be used to measure any specimen's birefringence, regardless of the orientation of the birefringence axis within the plane of focus.

The Pol-Scope also includes a CCD camera and specialized digital image-processing algorithms for producing images whose brightness for each pixel is strictly proportional to the birefringence retardation of the particular object point and is independent of its slow-axis orientation. Thus unlike conventional polarizing microscopes it provides a calculated birefringence-distribution map that has no blind direction, regardless of the orientation of the molecular or the fine-structure axes in the image plane. In addition to the magnitude the Pol-Scope also provides a map of orientation values of the birefringence axes in each image point.

The Pol-Scope measures the magnitude of birefringence as birefringence retardation, which represents the relative phase shift between the *e* and the *o* rays after they traverse the birefringent specimen. This phase shift is often expressed as a length in nanometers and is called retardance (the birefringence multiplied by the specimen thickness). The Pol-Scope measures the retardance in every resolved sample area simultaneously. The measured retardance maps are presented as images that show retardance values in shades of gray.

The microscope setup used for the Pol-Scope measurements is described in more detail in Ref. 14. The following is a list of instrument parts and settings employed in this study: We used a Nikon Model Microphot SA microscope that was equipped with a Model Apochromat, oil-immersion condenser lens with a NA of 1.4 and a 60×, 1.4-NA Model Plan Apochromat objective lens, both of which were selected for high extinction between crossed polarizers (all lenses were from Nikon, Inc., Melville, New York); a halogen lamp with frosted glass to illuminate homogeneously the back aperture of the condenser; a narrow-bandpass interference filter ($\lambda = 546$ nm with a 10-nm FWHM; Omega, Brattleboro, Vermont) for monochromatic illumination. We used a video-rate CCD camera (Dage/MTI, Michigan City, Indiana, Model 300-RC) with on-chip integration and a Model AG-5 frame-grabber board (Scion Corporation, Frederick, Maryland) for recording images with a typically better than 1% intensity noise.

In addition to calculated retardance maps, we also show images of the specimen when it is viewed directly between crossed circular polarizers. These images were recorded by use of the Pol-Scope setup with the universal compensator set to extinction so that it produced circularly polarized light.

For image acquisition, processing, and analysis, we used a public-domain digital imaging platform (NIH-Image, developed at the U.S. National Institutes of Health and available on the Internet at http://rsb.info.nih.gov/NIH-image), which we supplemented with custom-written software functions.

3. Results and Discussion

We recorded optical sections of calcite crystals by using high-NA lenses and a new type of PLM, the Pol-Scope (see Section 2). Crystals ranged in size from more than 8 μm in diameter to less than 0.1 μm.

Figure 1 shows optical sections of an 8-μm-diameter crystal viewed directly between crossed circular polarizers. The crystal morphology seen in the in-focus image corresponds to a projection of the cleavage form of calcite that is a rhombohedron. The crystal lies on one of its rhombohedron faces. The blunt corner of the crystal habit can be used to identify the direction of the optic axis that is oriented so that it makes equal angles of 45.5° with each of the three faces (Fig. 2). Hence the projection of the optic axis into a rhombohedron face bisects the obtuse angle of 102°. Furthermore, because one of these faces is normal to the microscope axis, the optic axis of the

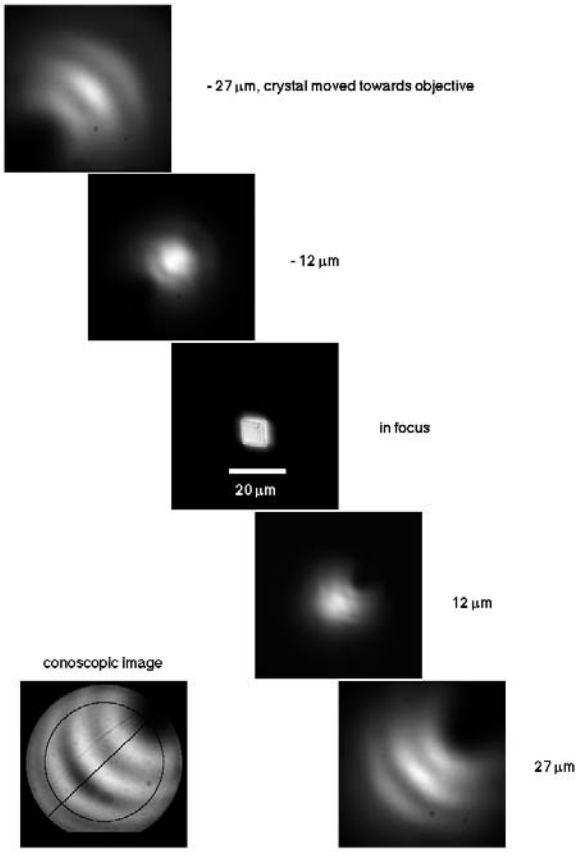

Fig. 1. Images of a calcite crystal imaged between crossed, circular polarizers by use of a Model Plan Apochromat oil-immersion objective with a NA of 1.4 and a condenser lens with the same NA. The crystal is embedded in a medium with a refractive index of 1.52. The diagonal series of images were taken in the orthoscopic mode with the crystal located in different z positions. The z positions are indicated by the labels to the right of each image (for positive z positions the crystal was moved away from the objective lens, whereas for negative z positions the crystal was moved toward the objective lens). At the bottom left-hand side the conoscopic crystal image is shown. The conoscopic image is superimposed by use of a black line that bisects the obtuse crystal face in the in-focus image and by a circle that corresponds to all the propagation directions that are tilted by 45° to the microscope axis in specimen space. The dark region near 1.5 o'clock of the conoscopic pattern is located at the intersection of the two curves and corresponds to the optic-axis direction of the crystal.

crystal makes an angle of 44.5° with the optic axis of the microscope.

The orientation of the optic axis of the calcite crystal is apparent in the conoscopic image shown on the bottom left-hand side of Fig. 1. The conoscopic image, which we recorded by placing a Bertrand lens in the imaging path of the microscope, appears in the back focal plane of the objective lens. Points in the back focal plane correspond to propagation directions in the specimen space.[15] Hence the point in the back focal plane that corresponds to the optic-axis direction is fixed by the intersection of two geometric curves: (1) the line that bisects the obtuse angle of the crystal face in the orthoscopic image and (2) the circle that corresponds to all propagation directions

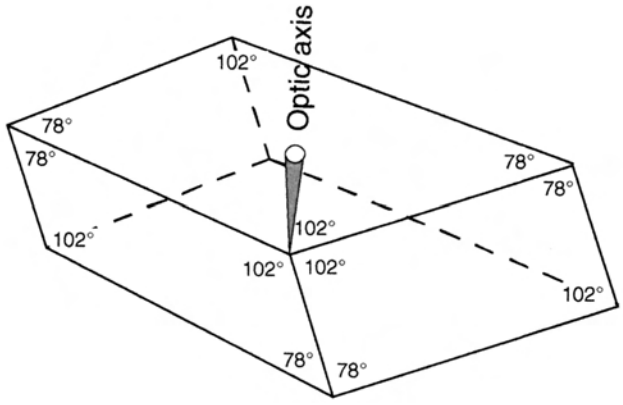

Fig. 2. Schematic diagram of the cleavage form of the calcite crystal that shows the face angles and the optic-axis direction.

that are inclined by 45° to the microscope axis in the specimen space. In Fig. 1 both loci are drawn into the image of the back focal plane and can be seen to intersect where the conoscopic intensity pattern shows a dark, ellipse-shaped area (near 1.5 o'clock of the conoscopic pattern). Light in that area propagates nearly parallel to the optic axis and will suffer little to no change in polarization. It is therefore extinct by the analyzer. In addition, as is expected, the line bisecting the crystal face constitutes a symmetry axis of the conoscopic pattern.

The bright and the dark circle segments in the intensity pattern of the conoscopic disk correspond to directions in the crystal that have equal inclinations to the optic axis of the crystal. Let us assume that the shape of the crystal is a sphere so that each ray that passes through the center of the crystal has the same physical path length, regardless of its inclination to the optic axis. Although the physical path length is the same, the optical path length changes with the inclination to the optic axis because of the change in refractive index for the e and the o rays. The retardance, i.e., the difference in the optical path lengths between the e and the o rays, increases steadily with increasing inclination of the rays to the optic axis. The crystal shown in Fig. 1 has a diameter of approximately 8 μm, which leads to an approximate maximum relative phase shift of 1400 nm ($=|\Delta n|d = 0.172 \times 8000$), or 2.6 orders of the 546-nm wavelength light used in our experiments. Hence there are three circle segments in the conoscopic pattern that are located between the dark spot representing the optic axis and the point opposite to it corresponding to a direction that is perpendicular to the optic axis.

We now turn to the out-of-focus images of the calcite crystal shown in Fig. 1. Apparently, the out-of-focus images become similar to the conoscopic image the further the crystal is moved away from the central, in-focus position. When the crystal is moved out of focus by somewhat more than 3 times its diameter in the direction away from the objective lens the out-of-focus image is almost indistinguishable from the conoscopic pattern. Furthermore, when

the crystal is moved by the same distance in the positive and the negative z directions the respective images are related by a point-symmetry operation, as is expected from the imaging properties of a compound microscope. These observations guided us in the analysis of the focus series of smaller calcite crystals whose conoscopic images cannot be observed. Small crystals produce conoscopic images that are too weak to be observed against the background light. Although, in the orthoscopic mode, the light that interacted with a small crystal is concentrated in the point-spread function, its conoscopic image is spread across the whole aperture and therefore is drowned in the noise of the background light.

Figure 3 shows Pol-Scope images of a calcite crystal whose optic axis is parallel to the microscope axis. The Pol-Scope images represent the measured magnitude of specimen retardances on a linear gray scale (see Section 2), in contrast to the squared relation between the intensity and the retardance when the specimen is observed between crossed circular polarizers.

The calcite crystal that is viewed along its optic axis shows little retardance in the in-focus Pol-Scope image. Only when the crystal is moved out of focus is the retardance that is associated with rays that have passed through the crystal at angles that are tilted with respect to the optic axis revealed. These results are in sharp contrast to the images that we recorded directly with the crystal placed between crossed circular polarizers. Those images show a much higher intensity when the crystal is in focus than when it is taken out of focus [Fig. 3(c)]. Apparently, light rays that superimpose at the same point of the in-focus image have passed through the crystal at different inclinations to the optic axis. Hence these rays have polarizations that differ among each other in ellipticity and axis orientation. Furthermore, these rays come from different points in the front focal plane of the condenser and are incoherent to each other. Therefore their superposition leads to a partial depolarization of the light that forms the in-focus image points. The partially depolarized light passes the analyzer and forms the bright image of the crystal that is placed between crossed circular polarizers. The partially depolarized light, however, does not contribute to the retardance measured in Pol-Scope images.

We also recorded optical sections of small calcite crystals with unresolved morphology. The size of these crystals is close to the resolution limit of the imaging system. For small crystals images were recorded at proportionately smaller z intervals (0.8 μm). The series of images at different z positions shows the same characteristic features as for the larger crystals.

Figure 4 shows a crystal with its optic axis nearly parallel to the microscope axis. The in-focus and the out-of-focus Pol-Scope images display the retardance pattern arranged circularly about the optic axis. Similarly to the images of the larger crystal shown in Fig. 3, we can recognize the partial depolarization of the light in the in-focus image by comparing the direct view of the crystal placed between circular polarizers to the retardance image of the crystal in the in-focus and the out-of-focus positions.

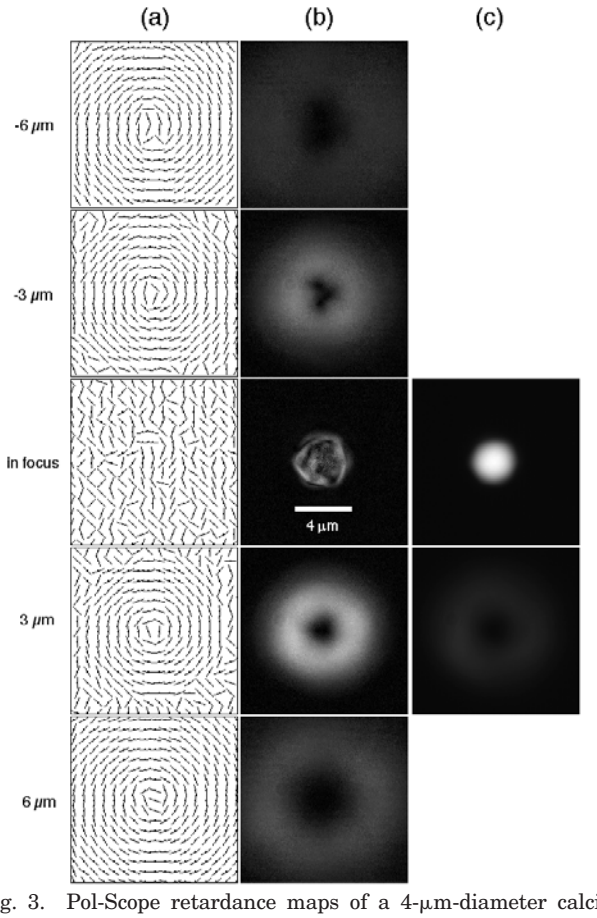

Fig. 3. Pol-Scope retardance maps of a 4-μm-diameter calcite crystal whose optic axis lies parallel to the microscope axis. The focus series of Pol-Scope images shows (a) the measured orientation of the birefringence axis and (b) the retardance magnitude. In the gray-scale images of (b) the white areas correspond to a 13-nm retardance and the black areas to zero retardance. From the orientation images of (a), one can see short lines that indicate the slow-axis orientations at regular grid locations. The birefringence pattern in the out-of-focus images is circularly symmetrical about the optic axis of the crystal. Rays that have traveled parallel to the optic axis form the dark center of the donut-shaped pattern. With increasing distance to the center the rays are more inclined toward the optic axis, the corresponding crystal retardance increases, and its slow-axis direction is perpendicular to the optic axis. Remarkable is the very reduced retardance measured in the in-focus image of the crystal. For comparison, in (c) we show the crystal image when viewed directly between crossed, circular polarizers. The in-focus image shows a very bright crystal, whereas in the out-of-focus image the light is spread over a larger area and is therefore much dimmer.

Figure 5 shows a submicroscopic crystal whose out-of-focus images display a clear asymmetry in their retardance distribution. For positive out-of-focus, or z, positions the pattern lacks retardance near the bottom, whereas for negative z positions the pattern lacks retardance near the top. Apparently, this submicroscopic crystal has an optic axis that is tilted

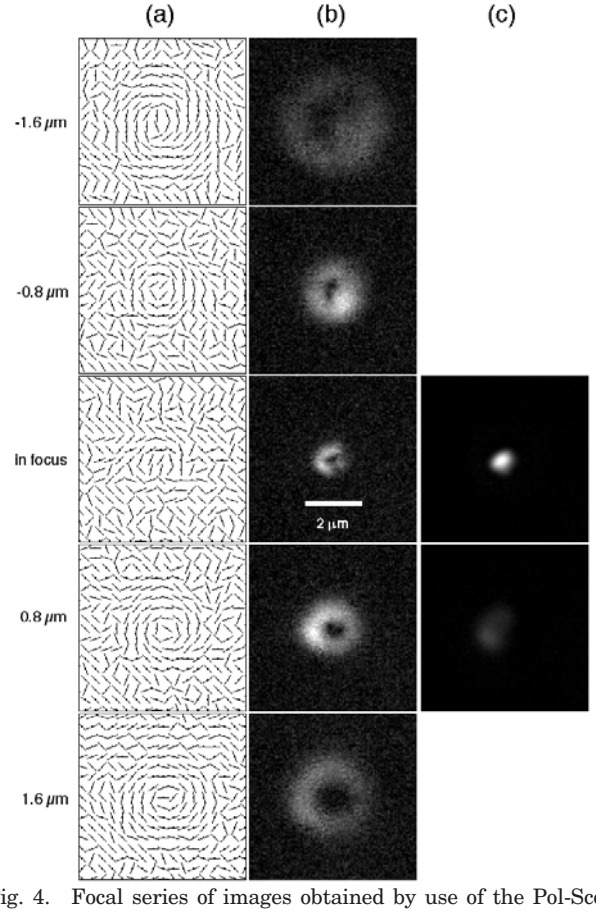

Fig. 4. Focal series of images obtained by use of the Pol-Scope retardance maps of a submicrometer-sized calcite crystal whose optic axis is nearly parallel to the microscope axis: (a) The measured orientation of the birefringence axis, (b) the magnitude of the retardance, (c) the crystal image when viewed directly between crossed, circular polarizers. Qualitatively, the same image features are observed in this small calcite crystal as are seen in the images of the larger crystal shown in Fig. 3. In (b) the white areas indicate a 3-nm retardance.

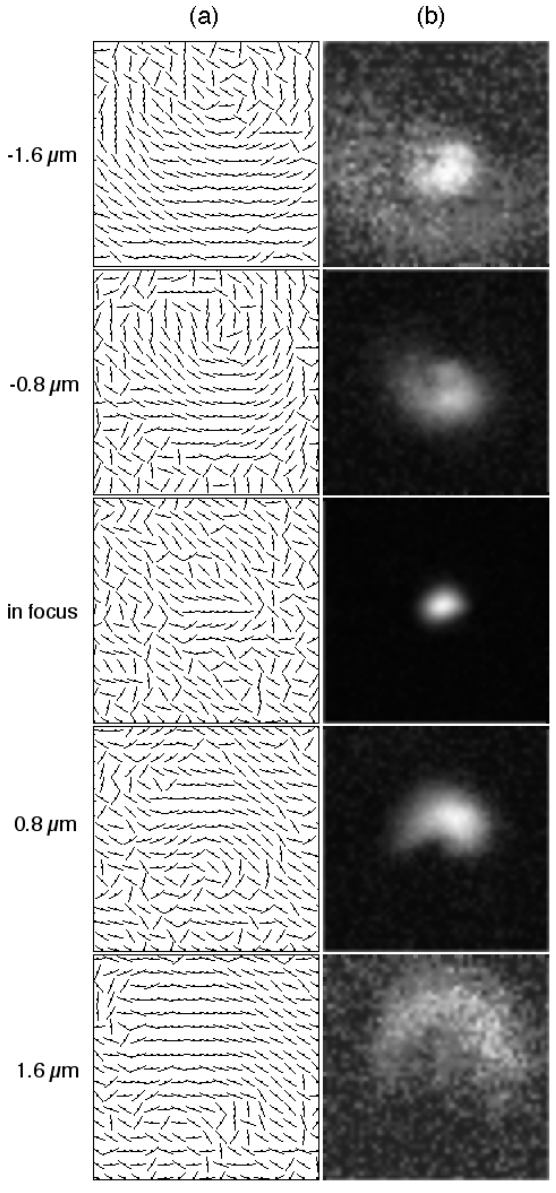

Fig. 5. Focal series of images of the retardance maps of a submicroscopic calcite crystal with an approximately 100-nm diameter (as estimated from the measured crystal retardance) that was imaged with the Pol-Scope: The asymmetrical distributions of (a) the birefringence-axis orientation and (b) the magnitude in the out-of-focus images indicate that the optic axis is tilted toward the microscope axis by approximately 45°. The magnitude images were contrast enhanced such that the maximum retardance decreases from 10 nm (white areas) in the in-focus image to 2 and 1 nm in the 0.8-μm and the 1.6-μm z positions, respectively.

with respect to the microscope axis, and the tilt direction leads to a projection of the optic axis that is oriented close to vertical in the image plane. By analogy to Fig. 1 it seems likely that the crystal's morphology is the cleavage form of calcite with a tilt angle of nearly 45° between the optic axis and the microscope axis. However, to identify unambiguously the tilt angle and the direction of the optic axis requires a more detailed analysis of the retardance-distribution maps.

The out-of-focus retardance maps shown in Figs. 4 and 5 exhibit some irregularities that seem to be associated with aberrations in the imaging system. For example, in Fig. 5 images for negative z positions of the crystal show a spot of high retardance that is centrally located in the pattern. Images for positive z positions, however, don't display this spot. We speculate that some of these irregularities are caused by birefringent inclusions and strain and stress patterns in the condenser and the objective lenses. Also, spherical aberration might contribute to retardance features that appear different at positive- and negative-focus positions. This spurious birefringence can possibly be identified by (1) a better characterization of submicroscopic crystals in their morphology by use of, e.g., scanning electron microscopy and (2) a comparison of experimental images with simulated images that were computed by use of an appropriate theoretical model of the imaging setup.

Therefore, to aid in the interpretation of the exper-

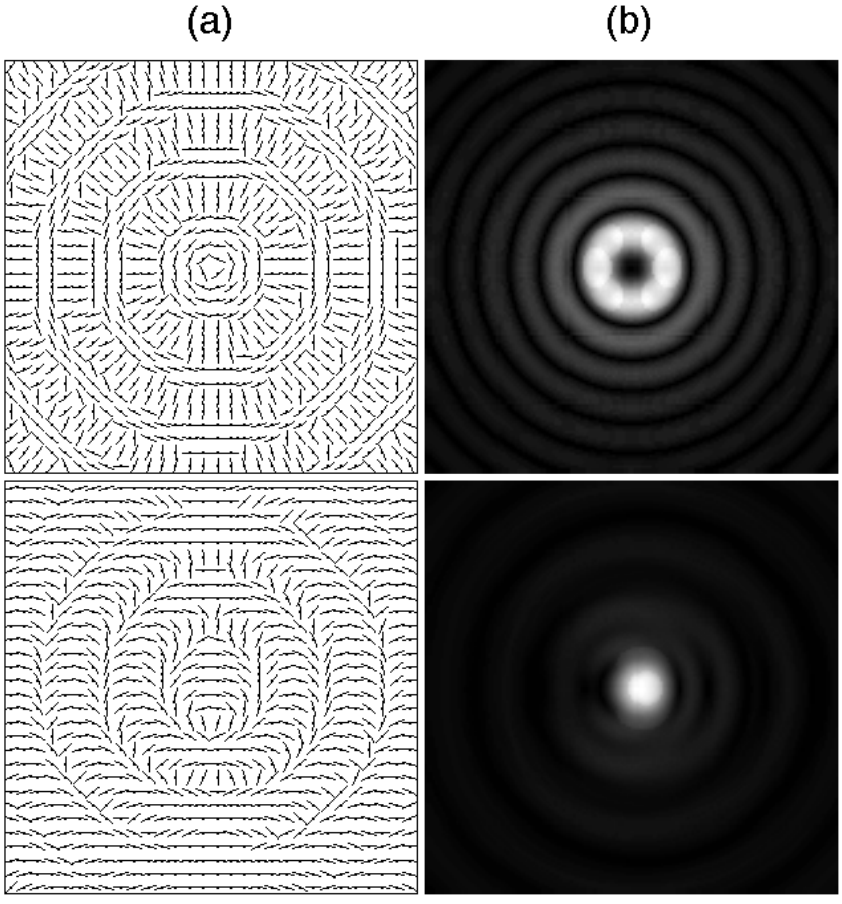

Fig. 6. Simulated Pol-Scope retardance maps of an anisotropic scatterer: (a) The orientation of the birefringence axis and (b) the magnitude of the retardance. The images are based on a vectorial theory of polarized-light imaging by use of high-NA lenses. The top images were calculated for a uniaxial scatterer with its optic axis parallel to the microscope axis, whereas the bottom images were calculated for an optic axis that was tilted by 45° in the vertical direction. The width of each image corresponds to 4 μm in specimen space.

imental results, we calculated simulated images of an anisotropic point scatterer by using a vectorial theory for high-NA imaging.[11] The theory models the Pol-Scope optical setup, including the polarizer, the analyzer, and the variable retarders that are used to measure specimen retardances. The scatterer is placed in the focal point of the imaging lens. For obtaining simulated Pol-Scope images, we first calculated theoretical intensity maps by assuming four different settings of the variable retarders. The four retarder settings corresponded to the settings that were used for recording experimental images.[10] Subsequently, the intensity images were combined to obtain the retardance magnitude and the orientation maps, again by use of the same algorithms that we use for experimental images.

Figure 6 shows simulated Pol-Scope images of an anisotropic point scatterer. The scatterer was represented by a tensor with dielectric coefficients that were derived from the calcite refractive indices. The two simulated images shown in Fig. 6 were calculated for two orientations of the tensor axis that corresponded closely to the optic-axis tilts of the images of the crystals shown in Figs. 4 and 5.

The images shown in Fig. 6 are in good agreement with their respective experimental counterparts of Figs. 4 and 5. One noticeable difference in the synthetic images is the appearance of rings surrounding the central maxima. We interpret the rings as diffraction phenomena that seem to be absent in the experimental images, even in images of crystals that had sizes seemingly below the resolution limit of the imaging system. In contrast, images of submicroscopic rodlike particles, which we published in an earlier paper,[14] showed detectable subsidiary maxima that we attributed to diffraction phenomena. In the images of the rodlike particles, we measured a central retardance line that was flanked by two parallel lines of lower retardance. The apparent birefringence axis was parallel to the rod in the central maximum but was perpendicular to the rod in the subsidiary maxima. This 90° flip in the axis direction in consecutive diffraction orders can also be recognized in the images of Fig. 6. It remains to be explored why the current experimental images of small calcite crystals do not show any detectable diffraction features.

4. Conclusion

We have recorded optical sections of calcite crystals to evaluate the basic features of the point-spread functions of submicroscopic birefringent objects imaged with the Pol-Scope. We have verified that the measured retardance distribution in out-of-focus images of small crystals is modulated by the orientation of the optic axis in the crystals. We conclude that the modulation can be used to determine the orientation of the optic axis of even unresolved, submicroscopic crystals.

We would like to thank Shinya Inoué of the Marine Biological Laboratory, Woods Hole, Massachusetts, for insightful discussions and a careful reading of the manuscript. P. Török is an Advanced Fellow of the Engineering and Physical Sciences Research Council at the University of Oxford, Oxford, UK. This research was funded by National Institutes of Health grant GM49210, which was awarded to R. Oldenbourg.

References

1. G. Mei and R. Oldenbourg, "Fast imaging polarimetry with precision universal compensator," in *Polarization Analysis and Measurement II*, D. H. Goldstein and D. B. Chenault, eds., Proc. SPIE **2265,** 29–39 (1994).
2. Y. Otani, T. Shimada, T. Yoshizawa, and N. Umeda, "Two-dimensional birefringence measurement using the phase shifting technique," Opt. Eng. **33,** 1604–1609 (1994).
3. M. Shribak, Y. Otani, and T. Yoshizawa, "Return-path polarimeter for two dimensional birefringence distribution measurement," in *Polarization: Measurement, Analysis, and Remote Sensing II*, Proc. SPIE **3754,** 144–149 (1999).
4. B. Wang and T. C. Oakberg, "A new instrument for measuring both the magnitude and angle of low level linear birefringence," Rev. Sci. Instrum. **70,** 3847–3854 (1999).
5. G. Yao and L. V. Wang, "Two-dimensional depth-resolved Mueller matrix characterization of biological tissue by optical coherence tomography," Opt. Lett. **24,** 537–539 (1999).
6. D. A. Agard, Y. Hiraoka, P. Shaw, and J. W. Sedat, "Fluorescence microscopy in three dimensions," in *Methods of Cell Biology*, D. L. Taylor and Y.-L. Wang, eds. (Academic, San Diego, 1989), Vol. 30, pp. 353–377.
7. S. F. Gibson and F. Lanni, "Experimental test of an analytical model of aberration in an oil-immersion objective lens used in three-dimensional light microscopy," J. Opt. Soc. Am. A **9,** 154–166 (1992).
8. L. Tao and C. Nicholson, "The three-dimensional point spread functions of a microscope objective in image and object space," J. Microsc. **178,** 267–271 (1995).
9. P. Török, S. J. Hewlett, and P. Varga, "The role of specimen-induced spherical aberration in confocal microscopy," J. Microsc. **188,** 158–172 (1997).
10. R. Oldenbourg and G. Mei, "New polarized light microscope with precision universal compensator," J. Microsc. **180,** 140–147 (1995).
11. P. Török, "Imaging of small birefringent objects by polarised light conventional and confocal microscopes," Opt. Commun. **181,** 7–18 (2000).
12. E. Hecht, *Optics*, 3rd ed. (Addison-Wesley, Reading, Mass., 1998).
13. R. Oldenbourg, "A new view on polarization microscopy," Nature **381,** 811–812 (1996).
14. R. Oldenbourg, E. D. Salmon, and P. T. Tran, "Birefringence of single and bundled microtubules," Biophys. J. **74,** 645–654 (1998).
15. S. Inoué and R. Oldenbourg, "Microscopes," in *Handbook of Optics*, M. Bass, ed. (McGraw-Hill, New York, 1995), Vol. 2, pp. 17.1–17.52.